



Why FETs detect a THz signal at a frequency far beyond their amplifying capabilities

Jacek Marczewski^{1*} , Michał Zaborowski¹ , Daniel Tomaszewski¹ ,
Przemysław Zagrajek² , Norbert Pałka² 

¹ Institute of Microelectronics and Photonics, Lukaszewicz Research Center, al. Lotników 32/46, 02-668 Warsaw, Poland

² Institute of Optoelectronics, Military University of Technology, ul. gen. S. Kaliskiego 2, 00-908 Warsaw, Poland

Article info

Article history:

Received 14 May 2024

Received in revised form 08 Aug. 2024

Accepted 28 Aug. 2024

Available on-line 02 Oct. 2024

Keywords:

Terahertz detection;
field-effect transistors;
Dyakonov-Shur theory;
resistive mixing;
surface plasmons.

Abstract

Field-effect transistors (FETs) are efficient detectors of THz radiation. Despite over three decades of research, controversy still exists regarding the detection mechanism. The article attempts to solve this problem systemically. Existing approaches to modeling THz detection are critically reviewed, including plasmonic, resistive mixing, hot carrier and thermal models. Limitations and inconsistencies of the first two approaches, along with some classical physics principles and experiments conducted, were identified. These include the facts that some models were formulated independently of material relaxation time constraints, and the plasmonic approach does not take into account the conditions for the formation of surface plasmon-polarons and does not describe the case of p-type devices (hole plasmons have never been experimentally recorded). Relevant measurements and theoretical considerations illustrate the inadequacy of these models. As a result of this analysis, thermoelectric models are expected to explain THz sensing by FETs.

1. Introduction

The answer to the title question was first proposed in the Dyakonov and Shur (D&S) plasmonic model developed for high electron mobility transistors (HEMTs) [1] which are members of the field-effect transistor (FET) family. This model assumed that THz energy supplied between the FET source and the gate terminals excites a surface plasmon at the top of the gate-controlled part of the transistor channel filled with free electrons. Surface plasmons used in the D&S approach are quantized longitudinal surface electromagnetic waves located at the boundary of the plasma formed by free electrons in metals or heavily doped semiconductors and dielectrics or wide-bandgap semiconductors, as in the case of HEMTs. In line with this theory, the plasmons propagate towards the drain of the transistor with a velocity much higher than the electron velocity resulting from the longitudinal electric field in the channel. Therefore, the asymptotic limit of the frequency of plasmons, called the surface plasmon frequency, is much higher than the maximum frequency of

the FET operation predicted by a drift-diffusion (DD) model of electron transport in solids. This fact is confirmed experimentally. In the D&S model, the THz signal of angular frequency ω is transduced to the ω -dependent DC photovoltage induced at the open drain terminal.

Another widely accepted explanation for THz detection is the so-called resistive mixing (RM) theory, i.e., multiplication in the time domain of harmonic signals entering the FET gate and drain terminals [2]. Like the D&S model, the FET photoresponse is a DC voltage induced at the open drain terminal (for DC). The RM model gained considerable attention, although it is limited to frequencies for which the classical transport model applies because it uses a simple compact model of the FET I-V DC characteristics. In the case of silicon FETs, this limits the validity of the RM model of the THz detection to frequencies well below 1 THz. However, it should be emphasized that efficient THz detection by Si FETs was observed even at frequencies above several THz [3].

Another mechanism that may be responsible for the THz detection in the FETs is a photothermoelectric effect, i.e., a transformation of the THz field energy into the electric signal at the device output. Such an approach was

*Corresponding author at: jacek.marczewski@imif.lukasiewicz.gov.pl

reported mostly in the case of graphene devices. Generation of the DC photovoltage in the gate-induced p-n junction was considered in Ref. 4. The device with multiple parallel separated graphene monolayers was considered in Ref. 5. The authors claimed that heating of the graphene layers by the absorbed radiation leads to thermoemission of carriers between the layers and finally to the generation of the DC photovoltage. Another thermal effect, i.e., generation of hot carriers was discussed in Ref. 6. Interestingly, more mechanisms were investigated to explain THz detection using graphene devices. Generation of the DC photoresponse based on the device characteristics nonlinearity was reported in Ref. 7. Plasmon-based models of electromagnetic radiation detection in graphene FETs were presented in Refs. 8 and 9. The authors of that approach claimed that plasmon resonances in a high-quality graphene monolayer were responsible for the photodetection. Such a variety of models of THz detection in graphene devices, although can be assigned to different device architectures, seems intriguing and requires further consideration.

Next, some attempts to identify a source of the THz detection in FETs using numerical simulations should also be mentioned. In Ref. 10, the Monte-Carlo (MC) solver of 2D Poisson and semi-classical transport equations, taking into account semiconductor band structure, quantum effects, and local electronic temperature, was used. Based on the simulations, the authors assigned peaks of the photocurrent visible at frequencies above 1 THz to the electron plasma oscillations. Moreover, they identified different oscillation modes in different parts of the HEMT channel. Similar simulations were presented in Ref. 11. The current photoresponse spectra were calculated according to the S-matrix terms. In addition, a quasi-static model expressed using terms of the DC drain current Taylor series expansion and S-parameters was developed. The simulations made in a broad range of frequencies showed consistency of both approaches only at frequencies up to hundreds of GHz. It was concluded that at the low frequencies, the THz detection is due to self-mixing of the AC signals inside the device whereas plasmons are responsible for the detection at high frequencies.

A brief review of the THz wave detection mechanisms discussed in the literature shows that, in our opinion, the question of which one is correct remains open and requires further studies. Knowledge of the mechanism is important for the design of detectors and understanding of their operation. In this paper, we try to contribute to the debate in the following sections. In section 2, we discuss the limits of a classic theory of charge carrier transport in semiconductors to directly consider possible THz detection mechanisms in FETs. To our knowledge, a similar discussion has not been presented so far in the works on detection modeling. In section 3, we present the experiments describing three types of tested FETs, accounting for the main differences between their architectures that can affect the photoresponse. The measured photovoltage characteristics with account for different channel conductivity types are presented and compared to emphasize similarities between the measurements despite significant differences between the FETs. Section 4 presents a more comprehensive discussion of the experimental data. This section also concerns a recently formulated thermoelectric model for silicon detectors [12], similar to the Seebeck effect often

referred to by researchers of graphene-based detectors [13, 14]. The concluding remarks are presented in the summary.

Since technologies for producing graphene-based devices are still in their infancy, the graphene-related experimental results will not be discussed, as several of them differ from each other. In this article, we do not discuss the idea of ballistic transport important only for very deep submicron transistors. In this case, the transport of carriers between the source and the drain is collision-free, which means that there is no maximum frequency limitation related to the relaxation time limit that will be discussed in section 2. It should also be mentioned that the photoelectric effect, sometimes mentioned in general works, does not apply to the HEMT and silicon detectors because the THz radiation quantum has low energy in relation to the width of the bandgap.

2. Fundamental limits of classical transport and plasmonic models describing THz detection

Many considerations regarding the mechanism of THz radiation detection by FET transistors are based on using the semi-classical charge carrier transport equations under the influence of an electric field. These are various approximations that largely simplify the more strict description based on the Boltzmann equation (1) illustrating changes in the carrier distribution function under the influence of external forces [15]:

$$\frac{\partial f}{\partial t} + \frac{\hbar \mathbf{k}}{m_{\text{eff}}} \cdot \nabla_{\mathbf{r}} f + \frac{d\mathbf{k}}{dt} \cdot \nabla_{\mathbf{k}} f = \left. \frac{\partial f}{\partial t} \right|_{\text{coll}}, \quad (1)$$

where f denotes the distribution of a single-particle position and momentum at a given time, \mathbf{r} is the generalized spatial coordinate, \mathbf{k} represents the wave vector, t is the time, and m_{eff} is the effective mass of a carrier. The right side of the equation corresponds to the effect of particle collisions. The Boltzmann equation and fluidic set of equations in the context of charge carrier transport exhibit the same constraints because the Boltzmann equation can be used to derive the fluid dynamic conservation laws for mass, charge, momentum, and energy [16]. The limitation of changes in the carrier velocity under the influence of a periodically changing electric field is related to the presence of a collision component [the term on the left side of (1)] describing the scattering of the free carriers. There are many scattering mechanisms, the most important of which, in the case of semiconductors, is scattering on phonons and free carriers. Scattering acts lead to the loss of the kinetic energy of carriers obtained from the electric field and, consequently, cause their inclusion in the pool of carriers in thermodynamic equilibrium. This phenomenon is described by the so-called carrier relaxation time [17], which is a function of the wave vector (and therefore energy) and the position of the electron (in the case of non-isothermal models). Then, using the relaxation time τ approximation, the scattering term can be expressed by (2):

$$\left. \frac{\partial f}{\partial t} \right|_{\text{coll}} = -\frac{f - f_0}{\tau}, \quad (2)$$

where f_0 denotes the Fermi-Dirac distribution function.

The concept of relaxation time is more general than the mean time between collisions because the carrier does not usually lose all of its excess energy in one act of collision. Generally, two types of limitations on the speed of transport phenomena in semiconductors should be considered: the carrier momentum relaxation time and its energy relaxation time. Both parameters determine the maximum frequency of changes in the electric field causing current flow. The limitations resulting from the relaxation time in the context of hydrodynamic transport models (which are simplifications of the Boltzmann equation) are discussed in more detail in Ref. 18. The experimentally measured energy and momentum relaxation times of electrons are of the same order for Si and GaAs – ca. 0.5 ps [19]. This fact limits the applicability of classical electron transport models in silicon or GaAs FETs to sub-THz or even lower frequencies. In the case of holes representing p-type channels, this limitation is stronger. It should be emphasized that these are material limitations of a fundamental nature, independent of the structure and operating principle of a specific detector.

Being widely represented in the literature on the interpretation of experimental works, the plasmonic model deserves a deeper analysis. It should be emphasized that the D&S model is based on electron phenomena and does not explain THz detection for p-type devices, although it is known that p-channel FETs (hole conduction) have very similar shapes of detection characteristics (see results of our experimental part) albeit with lower responsivity. We are not aware of any experimental reports on plasmons generated for free-hole gas that would need to be considered for p-type devices.

The surface plasmons are collective oscillations of electrons forming electromagnetic longitudinal surface waves at the interface between dielectric and electron plasma that might exist in semiconductors with sufficient concentration of free electrons [12]. Early works focused almost exclusively on plasmons excited at the metal-dielectric interface. The surface plasmons can interact with electromagnetic waves creating a coupled system called surface plasmon polariton (SPP). The dispersion of SPP can be found by solving Maxwell equations. SPP could exist only if the real part of the semiconductor complex dielectric function $\text{Re}(\varepsilon)$ becomes negative [20]. This effect could occur only well below the 3D plasma frequency ω_p . According to the widely accepted Drude theory (modified for semiconductors), the 3D plasma frequency is given by (3):

$$\omega_p^2 = \frac{n \cdot q^2}{\varepsilon_0 \cdot \varepsilon_\infty \cdot m_{\text{eff}}} - \frac{1}{\tau^2}, \quad (3)$$

where n is the concentration of free electrons, q is the elementary charge, ε_0 is the permittivity of vacuum, ε_∞ is the high-frequency dielectric constant of semiconductor, m_{eff} is the effective mass of electrons and τ is the momentum relaxation time representing a damping term. From a physical point of view, ε_∞ reflects the contribution of charges, the effective mass accounts for the band structure. The last term, containing τ , is often omitted in the considerations, which is an obvious mistake because, unlike for metals, for plasmons excited in semiconductors, the presence of collisions represented by τ significantly

reduces the ω_p value or even prevents the formation of plasma. Simple calculations performed for silicon show that for the electron density below a certain value, $n \sim 10^{17} \text{ cm}^{-3}$ as calculated using formula (1), the free-electron plasma resonance cannot occur (ω_p^2 becomes negative). Experimental measurements of the value of the complex dielectric function in silicon are possible using time-domain spectroscopy (TDS) over a wide range of THz frequencies. They can be used to confirm the impossibility of SPP formation in materials such as Si and GaAs at room temperature.

Another problem that should be addressed in any plasmonic theory is a method of coupling THz radiation with surface plasmons. This issue is not explained by the D&S theory, which is why many experimenters believed that it was sufficient to connect a THz antenna to the transistor to obtain a surface plasmon. The conditions for the excitation of surface plasmons are not trivial and can be found in textbooks on the interaction of solids with electromagnetic waves, e.g., [20]. It is impossible to couple THz radiation directly from the dielectric (air) into the SPP modes. Excitation of surface plasmons usually requires dedicated solutions in the form of, for example, a diffraction grating adjusting the plasmon and incident wave vectors or coupling with the plasmon component in the dielectric using a prism system. Examples include an experiment using a silicon n-channel transistor at helium temperature to excite surface plasmons using a diffraction grating [21].

The RM approach has even stronger limitations. It utilizes simple, compact models of DC I-V FET characteristics that multiply the THz signal provided through the gate and drain terminals. Such models were derived based on the drift-diffusion approach, the simplest approximation of the Boltzmann equation. Therefore, its limits at first glance are the same as for (1). However, even stronger limitations are imposed by the non-quasi-static behavior of the FET channel due to its distributed nature revealed at high frequencies order of hundreds of GHz.

3. Experimental

The experimental part of this work concerns measurements of the photoresponse of n- and p-channel FETs detectors at two frequencies: a lower one – 340 GHz to demonstrate similarities and differences in their photoresponse, and a higher one – 3.3 THz to show that THz detection also occurs at frequencies exceeding the limits of the classically understood carrier transport. We used p-channel devices in our experiments as well, because they are rarely reported in the context of THz detection, but they can be useful as a decisive argument in the discussion of the plasmonic detection mechanism.

The last part of the experiment involves measuring the dielectric function of moderately doped n- and p-type silicon. The results of this research indicate that for such carrier concentrations at room temperature, the formation of surface plasmons is not possible for this material.

Detectors were monolithically integrated with the antennas. Their DC properties (current characteristics as a function of gate and drain voltages relative to the source) have a very similar shape with obvious differences in the

form of mirror images of the characteristics for both types of channels.

The first detector under test was the junctionless field-effect transistor (JLFET), used occasionally in sensor technology. Its internal structure is similar to a classic FET, with the difference that the drain, channel, and source areas are made of silicon of the same type of conductivity (without p-n junctions) – Fig. 1(a). A JLFET channel is, unlike the channels of other FETs, a 3D object. The conduction of this detector is influenced by the gate potential, which, by repelling the majority of carriers from the gate electrode, narrows the conductive part of the channel until it is completely closed near the threshold voltage V_{th} . For such a gate bias, the concentration of free carriers in the depletion layer just below the gate is several orders of magnitude lower than for flatband conditions, where its value is determined technologically. Suitable simulations of carrier distribution for n-type JLFET are presented in Ref. 12. There, one can also find an n-type JLFET response measurement without an antenna, but using a special probe station.

The n- and p-channel JLFET detectors, equipped with patch antennas shown in Fig. 2 were fabricated using the silicon-on-insulator (SOI) technology. They had channel dimensions $W/L = 6 \mu\text{m}/4 \mu\text{m}$ and a channel thickness of 170 nm. The selection of such a device, characterised by the high channel resistance and quite large dimensions, allows to exclude D&S, ballistic, and RM mechanisms from our considerations (this will be analysed in detail in the discussion section).

The second device measured was a classic MOSFET with dimensions and antennas similar to the JLFET. The n- and p-channel MOSFETs were manufactured using the same technology. Such a device is a reference point for many publications on THz detection by silicon FETs. The MOSFET channel is a thin, quasi-2D inversion layer induced in the semiconductor by the gate potential [Fig. 1(b)]. As the gate voltage changes from inversion towards V_{th} , the concentration of free carriers in the channel decreases. Below V_{th} this change is exponential and results in lowering concentration beneath the gate by several orders of magnitude. The large dimensions of the device (in our case) exclude the phenomenon of ballistic transport, which is often mentioned when describing submicron FET THz detectors called TeraFETs.

The third device measured was a modern AlGaAs/GaAs pseudomorphic HEMT in which an electron-filled 2D potential well provides a high-conductivity channel [Fig. 1(c)]. Similarly to the MOSFET, the gate potential affects the conductivity of this device. The transistor was made using commercial technology (United Monolithic Semiconductors) with a 100 nm wide gate. The process provided a transition frequency (f_T) of 130 GHz, more than three orders of magnitude higher than the JLFETs and MOSFETs used in our experiment.

This transistor, monolithically integrated with a log-periodic antenna mounted on a silicon lens, shown in Fig. 3, served in our experiments as a reference point for D&S theory, which was originally developed for HEMTs. Although rarely reported in the literature, p-channel heterojunction field-effect transistors (called pHFETs) have not been investigated in the context of THz sensing.

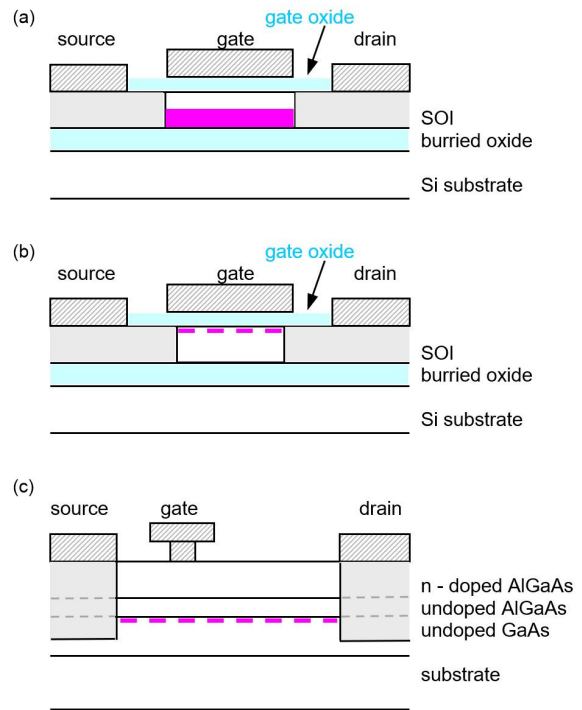


Fig. 1. Schematic cross-section of JLFET (a), MOSFET (b), and HEMT (c). Channels marked in magenta. Dashed lines indicate 2D channels.

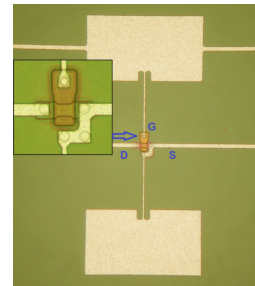


Fig. 2. A dual pad antenna integrated with JLFET. The transistor is shown in the inset.

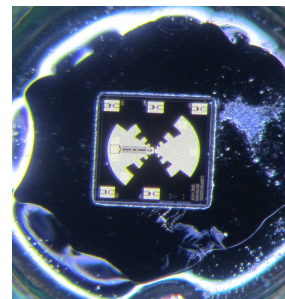


Fig. 3. Log-periodic antenna integrated with HEMT and glued to a Si lens.

The photoresponse of all mentioned detectors was measured. As a source of radiation, the frequency multiplier (from Virginia Diodes, Inc.) equipped with a diagonal horn antenna was used. For lock-in measurements, the radiation source was electronically modulated with a 187 Hz frequency, while for the voltmeter, the radiation was not chopped. To focus the divergent beam on the detectors, a refractive high-density polyethylene (HDPE) lens was

used. To measure the signal, both: a lock-in amplifier (SR830, Stanford Research) with an SR550 preamplifier and a sensitive voltmeter (PXI-4071, National Instruments) were used. The latter allowed to obtain information about the photovoltage sign. The measurement setup is shown in Fig. 4.

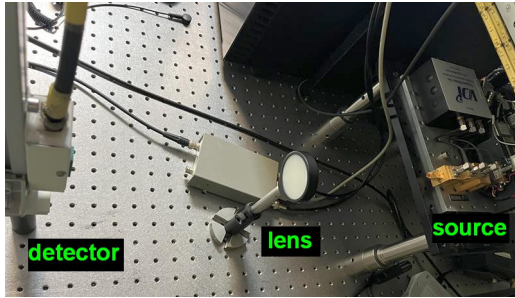


Fig. 4. Photo of the experimental setup with the source of radiation, the lens, and the detector.

The results of the measurements are shown in the following graphs in Figs. 5–7. For better readability, different colours (brown for p- and green for n- channel devices) of photovoltaic characteristics were used. Figure 5 shows THz detection (as the normalized photovoltage) by low-doped n- and p-type JLFETs – Figure 6 shows detection by n- and p-type metal-oxide-semiconductor FETs, (MOSFETs), and Figure 7 concerns an AlGaAs/GaAs HEMT. V_{th} , as marked on the figures, denotes the threshold voltage representing the cut-off of the channel, while V_{fb} represents the flat-band condition. The signal-to-noise (S/N) ratio during measurements ranged from 70 to 50 dB, except for p-MOSFET, for which the S/N value was much lower. The responsivity of n-type silicon devices was a single V/W, while the NEP was on the order of 10^{-9} W/Hz^{1/2}.

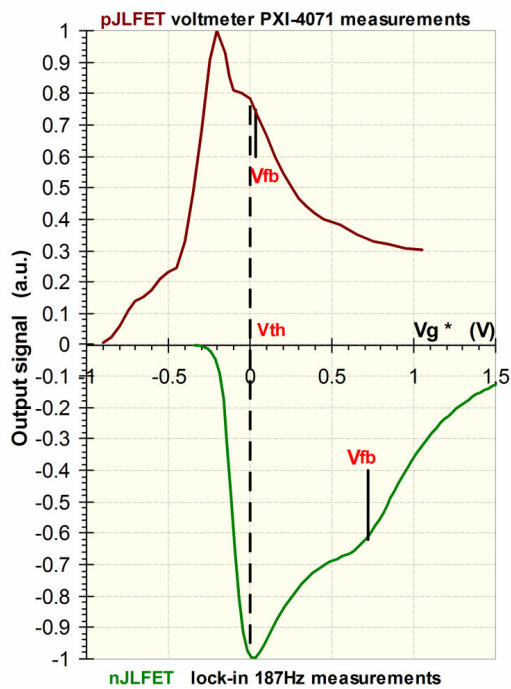


Fig. 5. Relative JLFET photoresponse $V_{out}/|V_{max}|$ as a function of the gate bias V_g^* defined for n-type detectors as $V_g - V_{th}$ and for p-type detectors as $V_{th} - V_g$. The V_{fb} and V_{th} biases are marked.

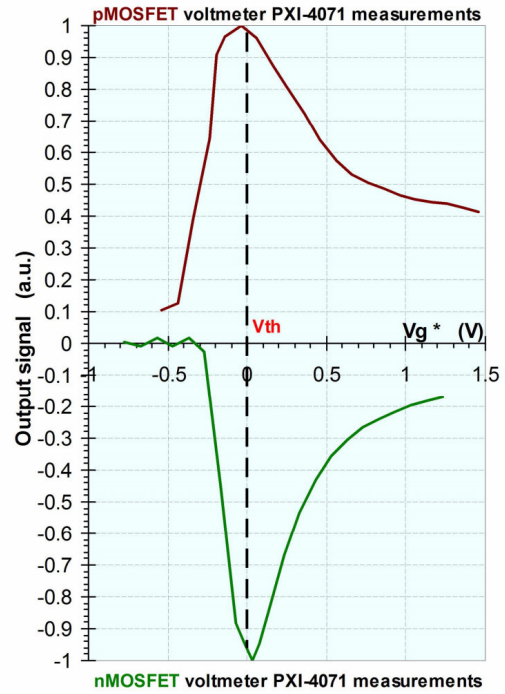


Fig. 6. Relative MOSFET photoresponse $V_{out}/|V_{max}|$ as a function of the gate bias V_g^* defined for n-type detectors as $V_g - V_{th}$ and for p-type detectors as $V_{th} - V_g$.

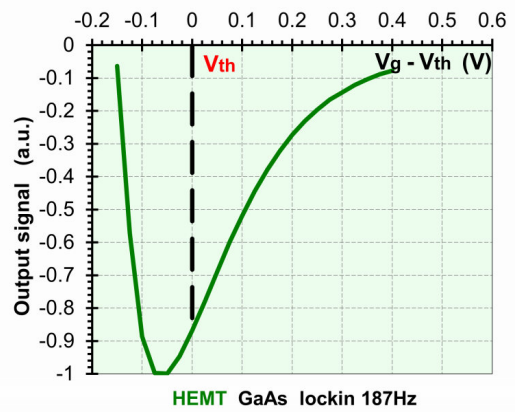


Fig. 7. Relative HEMT photoresponse $V_{out}/|V_{max}|$ as a function of the gate bias $V_g - V_{th}$.

As shown in Figs. 5–7, all devices show similar shapes of detection characteristics vs. the gate-source voltage (V_g) with the maximum sensitivity close to their threshold voltage (V_{th}). The threshold voltage has a different physical meaning (and sometimes a measurement method) for each transistor family being measured. In each case, it refers to the source-gate voltage V_g at which the channel becomes very resistive, and the carrier density in the channel is very low. Normalization of characteristics helps in comparing shapes of photoresponse, because p-channel detectors are less sensitive than n-channel ones, and the HEMT detector with incomparably smaller parasitic parameters outperforms the others in terms of sensitivity and S/N ratio.

All n-channel detectors examined in those experiments produced a negative photovoltage at the drain terminal (relative to the source), while THz radiation is delivered between the source and the gate. The gate was connected to the neutral point of the patch antenna. In contrast, all our

experiments performed on p-channel FETs (also described in Ref. 22), yielded a positive photoresponse. The same feature concerns the sign of the photocurrent measurements. The photovoltage sign was additionally confirmed using a sensitive voltmeter.

Although we performed measurements at 340 GHz, all described n-type detectors (equipped with log-periodic wideband antennas) can detect signals above 3 THz as was verified in another experiment concerning saturation of FET photoresponse published by members of our group [23].

In the high-frequency experiment mentioned above, the source of radiation based on a CO₂ laser was used. It was equipped with a gas chamber that converted 10 μm wavelength into the THz region. We obtained frequencies in the range of 0.6–3.3 THz depending on the gas that filled the chamber and its pressure. The beam from the source was divided into the first line detected by the reference detector and the experimental line contained an optical setup that finally directed the beam onto the investigated detector with a parabolic mirror. The signal from both detectors was collected with a digital oscilloscope. The laser operated with pulses of about 100 ns duration and with 1 Hz repetition rate. The radiation was linearly polarized.

All three families of n-channel FETs using the same antenna design, mounted on the flat part of the antenna lenses and measured with a trans-impedance amplifier, detected THz radiation at the highest available frequency of 3.3 THz. Their sensitivity, however, was degraded with increasing radiation frequency due to the influence of parasitic elements and the deterioration of antenna matching as expected [24]. The HEMT, fabricated in deep-submicron technology, had significantly higher responsivity (150 V/W at 0.18 THz) and lower noise equivalent power ($1.3 \cdot 10^{-11}$ W/Hz^{1/2}) than the silicon transistors.

The last part of the experiment consisted of measuring the real part of the dielectric function $\text{Re}(\epsilon)$ of single-crystalline silicon samples characterised by free carrier (holes and electrons) concentrations significantly greater than those found in the measured FET transistors for gate bias near the maximum of THz detection. These measurements aimed to experimentally determine whether the conditions necessary for the occurrence of plasmon effects used in the D&S theory can be met in silicon transistors at room temperature.

The carrier concentration in the measured samples was $2 \cdot 10^{15}$ cm⁻³ for the n-type sample and $3 \cdot 10^{15}$ cm⁻³ for the p-type. These numbers of free carriers significantly exceed the carrier density under the gate near the cut-off point (represented by V_{th}) of our silicon FETs. The dielectric properties of silicon samples in the THz range were analysed using time-domain spectroscopy employing a sophisticated optoelectronic system from TeraView, UK. The TDS setup used a femtosecond laser, photoconductive antennas, and a delay line to generate and accurately detect electromagnetic pulses lasting about 0.5 ps, covering a broad spectrum from approximately 0.1 to 3.0 THz. The samples were positioned at the focal point of the THz beam, and measurements were conducted under purged air conditions to minimize interference from atmospheric water vapour. Using a coherent detection scheme, this setup, operating in a transmission configuration, yielded both transmissive and dispersive data (the complex dielectric function) of the samples with a resolution of 10 GHz.

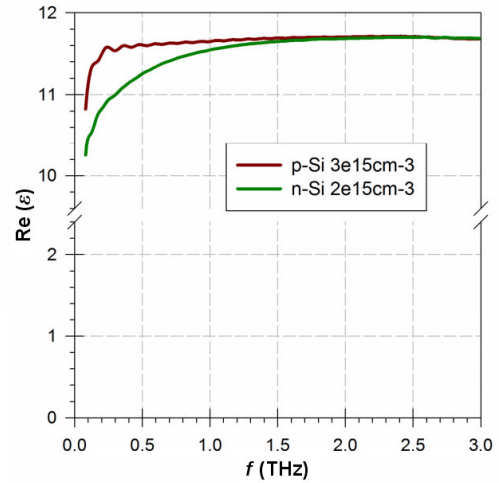


Fig. 8. Real part of dielectric function vs. frequency as measured by TDS for boron- and phosphorus-doped silicon. The concentration of carriers is $2 \cdot 10^{15}$ cm⁻³ and $3 \cdot 10^{15}$ cm⁻³, respectively.

The results shown in Fig. 8 prove that the number of free carriers, even for much higher concentrations than those for threshold voltage, is insufficient to balance the polarizability associated with the bound electrons, which is a necessary condition for forming SPP. This fact is indicated by only a slight downward bend of both characteristics in the sub-THz range. For our measurement frequency (340 GHz), the $\text{Re}(\epsilon)$ value decreases by only one percent for the p-type sample and by about 6% for the n-type sample compared to the value for 3 THz (it does not reach negative values required by plasmonic theory).

4. Discussion

In our opinion, there is a common mechanism of detection for all FETs. It should be included in one coherent theory valid for both p- and n-type FETs, explaining the sign of photoresponse, as well as the fact of their fast detection exceeding several THz. The argument in favour of this thesis is the fact that the detection characteristics are very similar for both n- and p-channel devices, regardless of the very different operating principles of the specific transistor family and their channel material (Si, GaAs). The authors are aware that several scientists suggest that there are two independent but compatible THz detection mechanisms for lower and higher frequencies, e.g., [14, 25], but the consistency of detection results together with the identified material and design constraints in our experiments contradict this.

The RM model is not a candidate for one coherent theory because it cannot be used for frequencies higher than those limited by classical transport. Classic models of free carrier transport under the influence of an electric field, including advanced versions of the Boltzmann equation (fluidic models and MC approaches), assume that the collision probability depends on the average time between collisions (or viscosity term in the case of fluidic models). After several collisions, the carrier enters the carrier pool in thermal equilibrium. Therefore, the part of carriers inversely proportional to the relaxation time does not contribute to the total current, as was discussed in section 2. In the case of an alternating electric field (THz), the inverse

of this time is the upper limit of frequency at which the device described by the classical model must stop working. In a simple fluidic interpretation, a particle moving in a sufficiently viscous medium stops responding to sufficiently fast force fields.

In the case of our silicon FETs, considering the measured carrier mobility μ values of $500 \text{ cm}^2/\text{Vs}$ (roughly proportional to the momentum relaxation time) for the n-type devices (and much smaller for p-type devices), this fundamental limit is well below 1 THz. However, it should be pointed out that our n-type silicon JLFET and MOSFET were used also in the experiment described in Ref. 4, where they successfully detected a 3.3 THz laser signal (the frequency significantly higher than the limit) reproducing a nanosecond shape on top of the signal envelope.

Moreover, besides this fundamental limit, the multiplication of very fast signals in the time domain (RM theory) by very slow JLFETs (due to their fairly resistive channel – tens of $\text{k}\Omega$ in open state resulting in large RC constant and f_T of 100 MHz), is impossible.

Focusing on a plasmonic approach, the silicon JLFETs were characterized by a relatively low carrier concentration (technologically defined). For the n-channel device at flat-band conditions, the concentration of electrons was $2 \cdot 10^{16} \text{ cm}^{-3}$, and the hole concentration of $1 \cdot 10^{15} \text{ cm}^{-3}$ for the p-type device. The carrier concentration in the gate region near the semiconductor surface drops rapidly as the gate bias changes from V_{fb} towards V_{th} due to channel depletion, reaching several orders of magnitude smaller levels. For such values of carrier density and τ of the order of a fraction of picosecond, reaching the plasma resonance frequency is impossible, which is the initial condition for any plasmonic effects to occur.

We confirmed this fact experimentally by measuring the real component of the $\text{Re}(\varepsilon)$ of moderately doped n- and p-type silicon samples (see Fig. 8). The small reduction of the $\text{Re}(\varepsilon)$ value at the detection measurement frequency (340 GHz) is insufficient for any plasmonic effects that could occur only if the $\text{Re}(\varepsilon)$ value were negative. The smaller carrier concentrations (for the bias close to the threshold voltage) than those in TDS samples, mean that the observed reduction in the $\text{Re}(\varepsilon)$ value for low frequencies (Fig. 8) would be even smaller than those for the values obtained by TDS measurements (even imperceptible). Physically, it means that the number of free carriers is not sufficient to balance the polarizability associated with the bound electrons, and, therefore, the plasmon effects are excluded.

Similar conclusions result from the analysis carried out for our MOSFET transistors. According to a commonly used definition, at the threshold, the surface concentration of carriers constituting the inversion channel is equal to the volume concentration of carriers of the opposite sign in the substrate. Only after exceeding the threshold voltage do free electrons appear in the inversion layer. The strong THz detection below V_{th} contradicts the postulate of a high carrier concentration necessary for plasmonic detection. In this case, the number of free carriers in the inversion layer near the threshold voltage is insufficient for surface plasmon to occur. It should be mentioned that a silicon FET at helium temperature may have sufficiently high mobility electrons in the channel (but not at the threshold voltage) to form surface plasmons [21].

For HEMTs (the case of Fig. 7), a relatively high electron mobility and concentration of carriers can be achieved. Also, in this case, the minimum electron concentration needed to meet the condition necessary for forming a plasmon can be accessed using (1). In the case of HEMT, the surface plasmon frequency is much lower than ω_p because the role of the dielectric is played by a wide-bandgap semiconductor that has a relatively high dielectric constant. Plasmonic effects then require very high carrier mobility, which is available essentially at cryogenic temperatures [26] due to the significant scattering of electrons on optical phonons, which lowers electron mobility. The mobility μ is related to the relaxation time of the carriers by (4):

$$\mu = \frac{\tau q}{m_{\text{eff}}}, \quad (4)$$

where q is the elementary charge, m_{eff} is the effective mass of carriers, and τ is the momentum relaxation time.

The electrons in the channel of the measured AlGaAs/GaAs HEMT could reach higher mobility and a significantly higher concentration of electrons compared to the n-type JLFET and MOSFET but not at the threshold voltage when its potential well is nearly emptied of carriers. As shown in Fig. 7, the photovoltage signal shows significant detection at the threshold region where the number of free electrons goes to a negligible value.

The Seebeck thermoelectric effect usually mentioned in the context of graphene-based detectors, e.g., [14], maybe the right solution for some semiconductors, but it is based on a strong assumption of thermal equilibrium of heated carriers with the crystal lattice [27], which is not met for silicon. The induced voltage V is defined by (5):

$$V = (S_{\text{AB, hot}} - S_{\text{AB, cold}}) \cdot (T_{\text{e, hot}} - T_{\text{e, cold}}), \quad (5)$$

where $S_{\text{AB, hot}} - S_{\text{AB, cold}}$ denotes difference of two Seebeck coefficients related to the “hot” and “cold” junctions between materials A and B, whereas $T_{\text{e, hot}} - T_{\text{e, cold}}$ is the difference in carrier temperatures in “hot” and “cold” junctions.

The thermoemission-based model [12] derived without the assumption that the hot electron temperature is equal to the lattice temperature, is one-dimensional and in its current form was created for JLFETs in the flat-band state in the channel. Then the photoresponse is expressed by (6):

$$V = -V_{\text{bi}} \frac{\Delta T_{\text{e}}}{T_{\text{L}}}, \quad (6)$$

where V_{bi} is a built-in voltage of the junction, ΔT_{e} is the increase in the electron temperature in the “hot” region, and T_{L} is the temperature of the lattice. This model correctly predicts the sign and value of the photoresponse with a slight overestimation probably resulting from its one-dimensionality.

As it was proved in section 3, the n-channel FETs produce a negative photovoltage while p-channel FETs produce a positive photoresponse. The sign of the photoresponse is usually not analysed in experimental works because, in most laboratories, a lock-in technique is used.

A lock-in voltmeter multiplies the modulated input signal by the reference signal of the same frequency. The lock-in measurement procedure recovers both: the DC signal amplitude and the relative phase to the reference signal (losing in such a way information about the original sign of the input voltage before modulation). Authors also checked the photovoltage sign using a sensitive voltmeter for lock-in measurements. Currently, sensitive source measure units (SMU) enable measurements of the photovoltaic sign even for very small signals [28]. The consistency of the photovoltage sign with experiments in the context of many detailed models presented in the literature may ultimately eliminate part of them, which will be discussed in another current publication.

5. Conclusions

All tested FETs have a similar photovoltaic response shape as a function of gate bias, negative for n-channel devices and positive for p-channel devices.

The plasmonic D&S model cannot explain the detection of p-channel FETs. Hole-gas plasmons have never been experimentally observed.

The plasmonic model cannot be applied to the silicon transistors with their low electron mobility of carriers at room temperature. Plasmons require very high electron mobility, unattainable at room temperature for known bulk semiconductors (except InSb), and a high carrier concentration. These parameters are not achievable at room temperature near the threshold voltage of FETs (including HEMTs), where strong THz detection exists in all our experiments. Some important issues related to the coupling of THz radiation with the SPP (beyond the scope of this paper) are also missed in D&S theory.

The widely used resistive mixing theory is based on the classical transport model and, therefore, cannot be applied above a certain frequency due to the relaxation time limits. In the case of silicon devices, this limit is much lower than their ability to detect THz signals.

Due to the shortcomings of the D&S and RM theories and their inconsistencies with experiments, we believe that there is another mechanism behind THz wave detection, common for all types of FETs. We believe that a strong argument for this statement is a close similarity of the photoresponse vs. gate voltage characteristics for three families of FETs presented in this work.

The right answer to the question asked in the paper title may be thermoelectric models that assume the conversion of THz energy into heat and the resulting consequences.

Authors' statement

Research concept and design, J.M.; collection and assembly of data, M.Z., P.Z., and N.P.; data analysis and interpretation, J.M., N.P., and M.Z.; writing the article, J.M., D.T. with the entire team; critical revision of the article, D.T.; final approval of article, J.M.

Acknowledgements

J. Marczewski thanks J. Lusakowski for sharing an opinion about our manuscript and A. Siemion for critical reading of the manuscript. Publication financed by the

Polish state budget under the Minister of Education and Science program, under the name Polska Metrologia project no. PM/SP/0042/2021/1, financing amount: PLN 744 128, total project value: PLN 744 128.

References

- [1] Dyakonov, M. I. & Shur, M. S. Plasma wave electronics: Novel terahertz devices using two dimensional electron fluid. *IEEE Trans. Electron Devices* **43**, 1640–1645 (1996). <https://doi.org/10.1109/16.536809>
- [2] Öjefors, E., Pfeiffer, U. R., Lisauskas, A. & Roskos, H. G. A 0.65 THz focal-plane array in a quarter-micron CMOS process technology. *IEEE J. Solid-State Circuits* **44**, 1968 (2009). <https://doi.org/10.1109/JSSC.2009.2021911>
- [3] Boppel, S. *et al.* CMOS integrated antenna-coupled field-effect transistors for the detection of radiation from 0.2 to 4.3 THz. *IEEE Trans. Microw. Theory Tech.* **60**, 3834–843 (2012). <https://doi.org/10.1109/TMTT.2012.2221732>
- [4] Castilla, S. *et al.* Fast and sensitive terahertz detection using an antenna-integrated graphene pn junction. *Nano Lett.* **19**, 2765–2773 (2019). <https://doi.org/10.1021/acs.nanolett.8b04171>
- [5] Ryzhii, V. *et al.* Graphene vertical hot-electron terahertz detectors. *J. Appl. Phys.* **116**, 114504 (2014). <https://doi.org/10.1063/1.4895738>
- [6] Cai, X. *et al.* Sensitive room-temperature terahertz detection via the photothermoelectric effect in graphene. *Nature Nanotech.* **9**, 814–819 (2014). <https://doi.org/10.1038/nnano.2014.182>
- [7] Auton, G. *et al.* Terahertz detection and imaging using graphene ballistic rectifiers. *Nano Lett.* **17**, 7015–7020 (2017). <https://doi.org/10.1021/acs.nanolett.7b03625>
- [8] Ryzhii, V., Otsuji, T. & Shur, M. Graphene based plasma-wave devices for terahertz applications. *Appl. Phys. Lett.* **116**, 140501 (2020). <https://doi.org/10.1063/1.5140712>
- [9] Caridad, J. M. *et al.* Room-temperature plasmon-assisted resonant THz detection in single-layer graphene transistors. *Nano Lett.* **24**, 935–942 (2024). <https://doi.org/10.1021/acs.nanolett.3c04300>
- [10] Mateos, J. & Gonzalez, T. Plasma enhanced terahertz rectification and noise in InGaAs HEMTs. *IEEE Trans. Terahertz Sci. Technol.* **2**, 562–569 (2012). <https://doi.org/10.1109/TTHZ.2012.2209970>
- [11] García-Sánchez, S. *et al.* Analysis of the THz responsivity of AlGaIn/GaN HEMTs by means of Monte Carlo simulations. *IEEE Trans. Electron Devices* **71**, 4556–4562 (2024). <https://doi.org/10.1109/TED.2024.3413713>
- [12] Marczewski, J., Tomaszewski, D., Zaborowski, M. & Bajurko, P. Thermoemission-based model of THz detection and its validation-JLFET case studies. *IEEE Trans. Terahertz Sci. Technol.* **12**, 633–647 (2022). <https://doi.org/10.1109/TTHZ.2022.3191836>
- [13] Hwang, E. H., Rossi, E. & Das Sarma, S. Theory of thermopower in two-dimensional graphene. *Phys. Rev. B* **80**, 235415 (2009). <https://doi.org/10.1103/PhysRevB.80.235415>
- [14] Ludwig, F. *et al.* Terahertz detection with graphene FETs: Photothermoelectric and resistive self-mixing contributions to the detector response. *ACS Appl. Electron. Mater.* **6**, 2197–2212 (2024). <https://doi.org/10.1021/acsaem.3c01511>
- [15] Mayr, J. The Boltzmann Equation and H-Theorem. https://www.thphys.uni-heidelberg.de/~wolschin/statsem21_4s.pdf (Accessed on July 15, 2024).
- [16] de Groot, S. R. & Mazur, P. *Non-Equilibrium Thermodynamics*. (New York: Dover Publications Inc., 1984).
- [17] Seeger, K. Relaxation Times in Semiconductors. in *Electronic Materials* (eds. Hannay, N. B. & Colombo, U.) 107–126 (Springer, Boston, 1973).
- [18] Yong, L. Relaxation time limits problem for hydrodynamic models in semiconductor science. *Acta Math. Sci.* **27**, 437–448 (2007). [https://doi.org/10.1016/S0252-9602\(07\)60044-7](https://doi.org/10.1016/S0252-9602(07)60044-7)
- [19] Palankovski, V. Bipolar Transistors. (Technischen Universität Wien, 2000). <https://www.ue.tuwien.ac.at/phd/palankovski/>
- [20] Fox, M. *Optical Properties of Solids. 2nd edition*. (Oxford Press, 2010).
- [21] Allen, S. J. Jr., Tsui, D. C. & Logan, R. A. Observation of the two-dimensional plasmon in silicon inversion layers. *Phys. Rev. Lett.* **38**, 980–983 (1977). <https://doi.org/10.1103/PhysRevLett.38.980>

- [22] Zaborowski, M., Marczewski, J., Tomaszewski, D. & Zagrajek, P. THz Detection in p-Type FETs. in *Proc. of 48th International Conference on Infrared, Millimeter, and Terahertz Waves (IRMMW-THz)* 1–2 (IEEE, 2023). <https://doi.org/10.1109/IRMMW-THz57677.2023.10299265>
- [23] Zagrajek, P. *et al.* Time resolution and dynamic range of field-effect transistor-based Terahertz detectors. *J. Infrared Milli. Terahertz Waves* **40**, 703–719 (2019). <https://doi.org/10.1007/s10762-019-00605-0>
- [24] Kopyt, P., Salski, B., Marczewski, J., Zagrajek, P. & Lusakowski, J. Parasitic effects affecting responsivity of sub-THz radiation detector built of a MOSFET. *J. Infrared Milli. Terahertz Waves* **36**, 1059–1075 (2015). <https://doi.org/10.1007/s10762-015-0188-y>
- [25] Roskos, H. G. *et al.* THz Detection with Field-Effect Transistors: The Role of Plasma Waves and of Thermoelectric Contributions. in *Proc. of 43rd International Conference on Infrared, Millimeter, and Terahertz Waves (IRMMW-THz)* 1–1 (IEEE, 2018). <https://doi.org/10.1109/IRMMW-THz.2018.8510444>
- [26] Bialek, M., Czapkiewicz, M., Wrobel, J., Umansky, V. & Lusakowski, J. Plasmon dispersions in high electron mobility terahertz detectors. *Appl. Phys. Lett.* **104**, 263514 (2014). <https://doi.org/10.1063/1.4886970>
- [27] Bulusu, A. & Walker, D. G. Review of electronic transport models for thermoelectric materials. *Superlattices Microstruct.* **44**, 1–36 (2008). <https://doi.org/10.1016/j.spmi.2008.02.008>
- [28] Paz-Martínez, G. P. *et al.* A closed-form expression for the frequency-dependent microwave responsivity of transistors based on the I–V curve and s-parameters. *IEEE Trans. Microw. Theory Tech.* **72**, 415–420 (2024). <https://doi.org/10.1109/TMTT.2023.3291391>